Geochemical Perspectives Letters

Molybdenum isotopes in plume-influenced MORBs reveal recycling of ancient anoxic sediments

Q. Ahmad[1*], M. Wille[1], C. Rosca[2], J. Labidi[3], T. Schmid[1], K. Mezger[1,4], S. König[5]

OPEN ACCESS

https://doi.org/10.7185/geochemlet.2236

Abstract

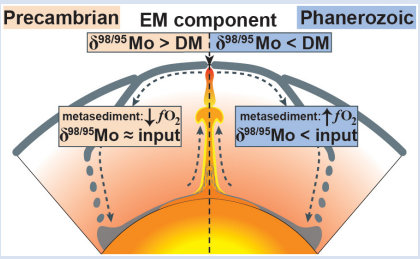

Under modern oxidising Earth surface conditions, dehydrated subducted slabs show Mo isotope compositions as low as $\delta^{98/95}$Mo = −1.5 ‰, compared to the depleted mantle $\delta^{98/95}$Mo = −0.2 ‰. Such light Mo isotope compositions reflect the redox-dependent aqueous mobility of isotopically heavy Mo associated with slab dehydration. Here we analysed basaltic glasses from the South-Mid Atlantic Ridge, whose parental melts are influenced by the enriched Discovery and Shona mantle plumes. We report increasingly higher $\delta^{98/95}$Mo of up to −0.1 ‰ from the most depleted samples towards those tapping more enriched mantle sources. $\delta^{98/95}$Mo values correlate with radiogenic Sr and Nd isotopes, which indicates the recycling of Proterozoic sediments with a Mo isotopic composition that was not affected by subduction-related, oxic dehydration. We propose that the Mo isotope signatures were retained during subduction and reflect anoxic conditions during deep sea sedimentation in the mid-Proterozoic. Finally, Mo isotope fractionation between different terrestrial reservoirs likely depends on the slab redox budget, and therefore on the timing of subduction with regard to Earth's surface oxygenation.

Received 28 April 2022 | Accepted 15 September 2022 | Published 12 October 2022

Introduction

The quantification of element and isotope fractionation in subduction zones plays an important role in understanding (re)cycling mechanisms between the Earth's surface and its interior over geologic time scales. Element and isotope fractionation in this setting can be controlled by the prevailing redox conditions of the subducted material. As aerobic conditions prevail at the Earth's surface today, deep sea sediments and altered oceanic crust (AOC) are largely oxidised and influence the redox budget of the subducting slab (*e.g.*, Evans, 2012). It is still unclear whether the redox budget of slabs is directly correlated with the oxygenation of Earth's atmosphere and oceans, and whether the redox state of the Earth's surface influences the behaviour of redox-sensitive elements in subduction zone settings through Earth's history.

A particularly suitable element to study the relationship between oxidised and reduced geochemical reservoirs is the redox-sensitive element Mo. The mobility of Mo from the subducted material is controlled by the redox state of slab-derived aqueous fluids and hydrous melts (Bali *et al.*, 2012; Skora *et al.*, 2017). Significant Mo mobilisation and isotope fractionation has been observed during subduction of oxidised lithologies, leaving behind a Mo depleted and isotopically light residual slab (*e.g.*, Freymuth *et al.*, 2015; König *et al.*, 2016; Chen *et al.*, 2019; Ahmad *et al.*, 2021). Under reducing conditions, only limited Mo mobility is expected to occur in subducted lithologies (Bali *et al.*, 2012; Skora *et al.*, 2017) thus preserving pre-subducted Mo signatures of the surface. This redox dependent mobilisation of Mo during subduction metamorphism potentially allows reconstructing the redox budget of ancient subduction zones through Mo isotope compositions of mantle-derived material enriched by ancient recycled crustal components.

This study investigates Mo isotope systematics in a well characterised basaltic sample suite from the South Mid-Atlantic ridge (S-MAR) that shows evidence for interaction with the enriched Shona and Discovery mantle plumes (Supplementary Information S-1, Fig. S-1). Previous studies on these samples suggested recycling of ancient oceanic crust and sediments in their mantle source with an age between 1 and 2 Ga based on radiogenic isotopes, and the absence of mass independent fractionation of S isotopes (Douglass *et al.*, 1999; Andres *et al.*, 2002; Labidi *et al.*, 2013). These basalts additionally feature increasingly heavier S and Se isotope compositions with indicators of mantle source enrichment, and are interpreted to reflect subduction recycling of reduced sediments from a redox stratified Proterozoic ocean (Labidi *et al.*, 2013; Yierpan *et al.*, 2020).

Results

The $\delta^{98/95}$Mo signatures of S-MAR basaltic glass samples range between −0.24 ‰ and −0.10 ‰. These $\delta^{98/95}$Mo values show

1. Institut für Geologie, Universität Bern, Baltzerstrasse 1+ 3, 3012 Bern, Switzerland
2. Fachbereich Geowissenschaften – Isotopengeochemie, Geo- und Umweltforschungszentrum, Eberhard Karls Universität Tübingen, Schnarrenbergstrasse 94-96, 72076 Tübingen, Germany
3. Université de Paris, Institut de Physique du Globe de Paris, CNRS, Paris, France
4. Center for Space and Habitability, Universität Bern, Gesellschaftsstrasse 6, 3012 Bern, Switzerland
5. Instituto Andaluz de Ciencias de la Tierra (IACT), CSIC & UGR, Avenida las Palmeras 4, Armilla, 18100 Granada, Spain

* Corresponding author (email: qasid.ahmad@geo.unibe.ch)

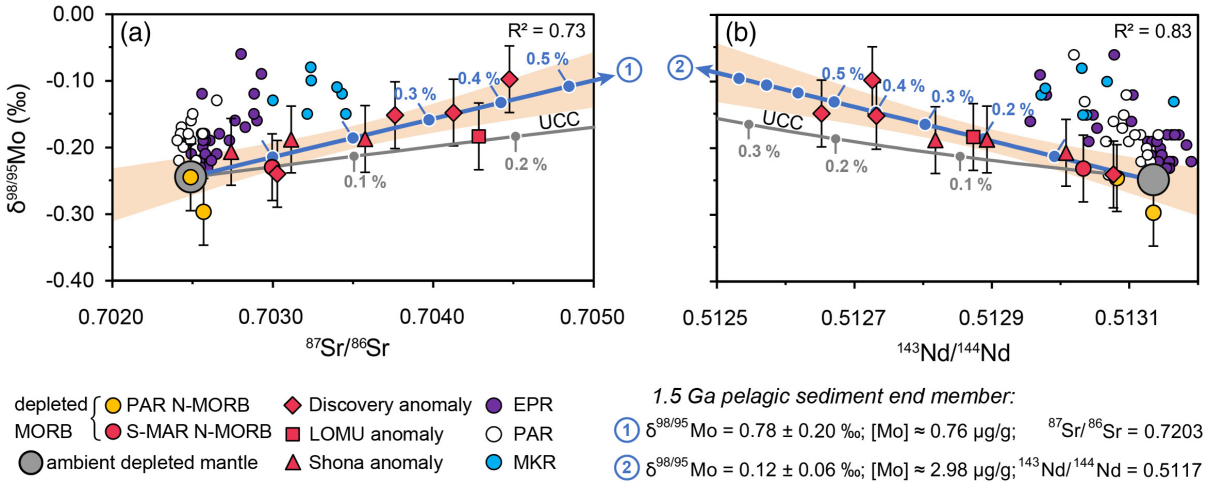

Figure 1 Covariation diagram of MORBs. **(a)** $\delta^{98/95}$Mo *vs.* $^{87}Sr/^{86}Sr$; **(b)** $\delta^{98/95}$Mo *vs.* $^{143}Nd/^{144}Nd$. Mixing of a 1.5 Ga old pelagic sediment end member (best fit parameters from linear regression) with the ambient depleted mantle (see Table S-2 for mixing parameters). Mixing with upper continental crust (UCC) is plotted for comparison. External reproducibility on each isotope value is considered for regression, and the shaded area indicates 95 % CI error envelope. PAR samples are excluded from regression. Error bars indicate 2 s.d. external reproducibility.

correlations with $^{87}Sr/^{86}Sr$ as well as $^{143}Nd/^{144}Nd$, $^{176}Hf/^{177}Hf$, and $\delta^{82/76}$Se (Figs. 1, S-4a,b). The correlations indicate that Mo isotopes trace mantle source enrichment. The range in $\delta^{98/95}$Mo of the samples is similar to that of MORBs (and seamounts) from the East Pacific Rise (EPR), the Pacific-Antarctic ridge (PAR), and the Mohns Knipovich ridge (MKR; Figs. 1, S-2). However, the samples from the S-MAR show a much larger variability in $^{87}Sr/^{86}Sr$ and $^{143}Nd/^{144}Nd$ and more systematic source enrichments (Figs. 1, S-2, S-4a,b).

Discussion

Origin of enriched mantle component. Combined element and isotope systematics of S-MAR samples strongly suggest that secondary mantle melting processes (such as sulfide melt segregation and fractional crystallisation), or seawater alteration, are unlikely the causes for the observed Mo isotope variations. This is because all these processes would have obliterated any correlation between Mo isotope composition and radiogenic isotopes (see Supplementary Information S-2 for further discussion). Low degree melting of mantle plume material has been suggested to affect geochemical signatures of investigated samples (le Roux *et al.*, 2002a), and might have affected their $\delta^{98/95}$Mo (*e.g.*, Chen *et al.*, 2022). We argue that this process did not result in a first order modification of the enriched source signatures of our samples. Their distinct radiogenic isotope compositions, their covariation with stable Se and S signatures, and trace element systematics are independent of partial melting variations, suggesting the plume source was enriched prior to low degree mantle melting (le Roux *et al.*, 2002a; Labidi *et al.*, 2013; Yierpan *et al.*, 2020). Moreover, the absence of a covariation of $\delta^{98/95}$Mo and Pb isotopes (Fig. S-4c,d) does not support the influence of an ancient low degree melt (Chen *et al.*, 2022). Rather, a recycled sediment component can explain the Pb isotope signature of LOMU-affinity samples (*cf.* Douglass *et al.*, 1999; Andres *et al.*, 2002). In addition, mantle melting degrees of 2.5 % (le Roux *et al.*, 2002a) cannot explain the observed variations of $\delta^{98/95}$Mo indicating that heavy Mo is likely a characteristic primary signature of the enriched plume material (see Supplementary Information S-2 for further details). Previous studies attributed this source enrichment to the influence of a recycled component, such as delaminated subcontinental lithospheric mantle, lower continental crust, or subducted sediment (±AOC) (Douglass *et al.*, 1999; Andres *et al.*, 2002; le Roux *et al.*, 2002b). In line with previous investigations showing covariations between other redox-sensitive stable Se-S isotope systematics and radiogenic isotopes (Labidi *et al.*, 2013; Yierpan *et al.*, 2020), we suggest that a sediment contribution to the S-MAR mantle source is the most likely scenario for the observed heavy Mo isotope enrichment in our samples (see Supplementary Information S-3 for further discussion). This sedimentary source was previously inferred to have a mid-Proterozoic age (1 to 2 Ga; Douglass *et al.*, 1999; Andres *et al.*, 2002; Labidi *et al.*, 2013; Yierpan *et al.*, 2020).

Mobility of Mo during subduction: the role of fO_2. Recycled Proterozoic sediments that enriched the S-MAR mantle source with isotopically heavy Mo are in stark contrast to inferred, isotopically light Mo in dehydration residues of subducted Phanerozoic metasediments (Ahmad *et al.*, 2021). The trend towards higher observed (co-) variations of $\delta^{98/95}$Mo with increasing degrees of mantle source enrichment within the S-MAR suite therefore implies recycling of a sedimentary $\delta^{98/95}$Mo or even a total Mo budget unaffected by dehydration and melting during subduction. This may be reconciled with experimental studies showing immobility of Mo in low fO_2-bearing slab fluids and hydrous slab melts (Bali *et al.*, 2012; Skora *et al.*, 2017; Chowdhury *et al.*, 2022). These experiments were conducted at subduction zone *P-T* and at reducing conditions, and showed that Mo^{4+} is immobile in fluids in the presence of rutile (Bali *et al.*, 2012) and mobilisation of Mo is inefficient in melts due to increased partitioning of Mo^{4+} relative to Mo^{6+} into the residual phases such as sulfides or rutile (Skora *et al.*, 2017; Chowdhury *et al.*, 2022). These findings are also consistent with subduction of organic matter (OM)-rich black shales in the Lesser Antilles Arc, where lavas south of Martinique exhibit high $\delta^{98/95}$Mo along with lower Mo/Ce (Freymuth *et al.*, 2016; Gaschnig *et al.*, 2017), suggesting the minute contribution of unfractionated slab-derived Mo to the mantle sources relative to melts originating from more oxidising sediments. Therefore, significant loss of heavy Mo during subduction metamorphism did not occur in the enriched mantle source component. This would have resulted in a preferential loss of more incompatible (isotopically heavy) Mo^{6+} during melting and dehydration (*e.g.*, Chen *et al.*, 2019; McCoy-West *et al.*, 2019) and would shift $\delta^{98/95}$Mo of the residual subducted material towards lighter values. The interpretation is in line with the fO_2-sensitive stable

Table 1 Average Mo isotope composition of MORBs from the S-MAR and PAR together with radiogenic isotope data (Douglass *et al.*, 1999) and Se isotope compositions (Yierpan *et al.*, 2020). Individual measurements are listed in Table S-1.

Sample	Type	$\delta^{98/95}$Mo (‰)[A]	*n*	$\delta^{82/76}$Se (‰)[B]	$^{87}Sr/^{86}Sr$	$^{143}Nd/^{144}Nd$
	Southern Mid-Atlantic ridge					
EW9309 40D-1g	Depleted N-MORB	−0.231	3	−0.18	0.702997	0.513033
EW9309 33D-1g	Discovery influenced MORB (North)	−0.098	3	−0.03	0.704475	0.512726
EW9309 28D-1g	Discovery influenced MORB (North)	−0.239	2	−0.14	0.703028	0.513077
EW9309 2D-1g	Discovery influenced MORB (South)	−0.148	2	−0.08	0.704127	0.512652
EW9309 4D-3g	Discovery influenced MORB (South)	−0.152	3	−0.04	0.703762	0.512732
EW9309 9D-3g	LOMU MORB	−0.183	2	−0.03	0.704284	0.512873
EW9309 15D-1g	Shona influenced MORB	−0.207	2	−0.13	0.702741	0.513008
EW9309 21D-1g	Shona influenced MORB	−0.188	2	−0.12	0.703115	0.512818
EW9309 22D-3g	Shona influenced MORB	−0.187	2	−0.08	0.703576	0.512893
	Pacific-Antarctic ridge					
PAC2 DR3 3-1	Depleted N-MORB	−0.245	3	−0.15	0.702488	0.513082
PAC1 CV-02g	Depleted N-MORB	−0.297	3	−0.23	0.702568	0.513135

[A] The external reproducibility (2 s.d.) is 0.05 ‰ (see Supplementary Information S-4).
[B] The external reproducibility (2 s.d.) is 0.08 ‰, except for EW9309 2D-1g and EW9309 9D-3g, for which it is 0.04 ‰ (Yierpan *et al.*, 2020).

isotope systematics of S and Se (Table 1), which indicate negligible mobilisation and isotope fractionation during subduction (Labidi *et al.*, 2013; Yierpan *et al.*, 2020). It is noteworthy that in some cases, that do not apply here, sediments may also buffer subduction zone fluids towards oxidising conditions, such as Fe- and Mn-rich (meta)sediments that show a high metamorphic fO_2 (Ague *et al.*, 2022 and references therein). Yet, our S-MAR data can be attributed to an immobile behaviour of Mo with unchanged $\delta^{98/95}$Mo under reducing conditions, which is in sharp contrast with the mobility of Mo under oxidising conditions where prograde subduction metamorphism can cause Mo mobilisation and alter the primary slab Mo isotope signature.

Recycled sediments from an anoxic deep ocean. The $\delta^{98/95}$Mo-$^{87}Sr/^{86}Sr$-$^{143}Nd/^{144}Nd$ covariations (Fig. 1) in the S-MAR data combined with the previously established model of the linear δ^{34}S-δ^{82}Se-$^{87}Sr/^{86}Sr$(-$^{143}Nd/^{144}Nd$) relationship (Labidi *et al.*, 2013; Yierpan *et al.*, 2020) allows extrapolation of $\delta^{98/95}$Mo and [Mo] to constrain the nature of the recycled sediment. Extrapolation of the linear regression to a model composition of 1.5 Ga old sediment ($^{87}Sr/^{86}Sr = 0.7203$, $^{143}Nd/^{144}Nd = 0.5117$; Fig. 1, see Table S-2 for details) yields two vastly different end member Mo signatures with $\delta^{98/95}$Mo of 0.78 ± 0.20 ‰ and 0.12 ± 0.06 ‰, and [Mo] of ~0.76 µg/g and 2.98 µg/g, respectively (see blue mixing lines in Fig. 1). This indicates that the linear extrapolation might not sufficiently constrain the Mo composition of the recycled sediment source. Considering the present day $^{87}Sr/^{86}Sr$ and $^{143}Nd/^{144}Nd$ model composition of 1.5 Ga old subducted sediment, the isotopic variations of the samples represents only a small fraction of the mixing space between the ambient depleted mantle and recycled sediment. Therefore, for given radiogenic Nd and Sr signatures of the sedimentary component, different $\delta^{98/95}$Mo and [Mo] combinations can potentially result in a minimum least squares error between the mixing model and the S-MAR data. As both variables cannot be independently constrained, a misfit function (Supplementary Information S-5) was applied to calculate the sedimentary $\delta^{98/95}$Mo and [Mo] that represent the measured $\delta^{98/95}$Mo-$^{87}Sr/^{86}Sr$-$^{143}Nd/^{144}Nd$ covariation best (Fig. 2).

Least squares errors for variable $\delta^{98/95}$Mo and [Mo] values for a given 1.5 Ga old sediment with $^{143}Nd/^{144}Nd$ and $^{87}Sr/^{86}Sr$ end member values (blue field in Fig. 2) show a similar pattern for both radiogenic isotope systems, which indicates that a mid-Proterozoic pelagic sediment is likely to be a valid end member. Best fits with minimum errors overlap with the lower 1σ of Proterozoic OM-rich sediment data from the literature (Ye *et al.*, 2021; Table S-2) and can also be achieved with a recycled sediment contribution close to that of the UCC (~0.05 to 0.15 ‰; Willbold and Elliott, 2017 and references therein) with slightly higher $\delta^{98/95}$Mo and/or [Mo] values. This points towards a minor authigenic Mo enrichment from seawater or a residual enrichment of Mo (*e.g.*, Kendall *et al.*, 2017) and implies that $\delta^{98/95}$Mo has not been affected by oxic conditions during slab dehydration due to subduction of reducing lithologies (Fig. 2).

These findings support the notion that the deep ocean remained anoxic until the beginning of the Phanerozoic (*e.g.*, Poulton and Canfield, 2011; Stolper and Keller, 2018). The extent of the biological pump in the Proterozoic ocean, where primary productivity in the oxygenated surface ocean was dominated by cyanobacteria, was lower compared to modern oceans and higher primary surface productivity was restricted to marine environments close to continents (Laakso and Schrag, 2019). This limited the OM flux to the Proterozoic deep ocean and therefore authigenic Mo accumulation from seawater. However, deep ocean anoxic conditions increased OM preservation and burial efficiency (Burdige, 2007). Furthermore, under anoxic conditions with an overall low concentration of dissolved SO_4^{2-} and MoO_4^{2-}, neither a significant Mo enrichment from seawater into the sediment nor a significant Mo mobilisation during fluid alteration is expected (Lyons *et al.*, 2014). The overall lower OM input to the deep ocean and smaller oceanic Mo reservoir can therefore explain the small authigenic heavy Mo contribution to the recycled mid-Proterozoic deep sea sediment (Fig. 2). With respect to the much shorter ocean residence time of Mo relative to the average lifetime of an oceanic crust, the S-MAR enriched end member is likely representative for overall reducing conditions during subduction and an average

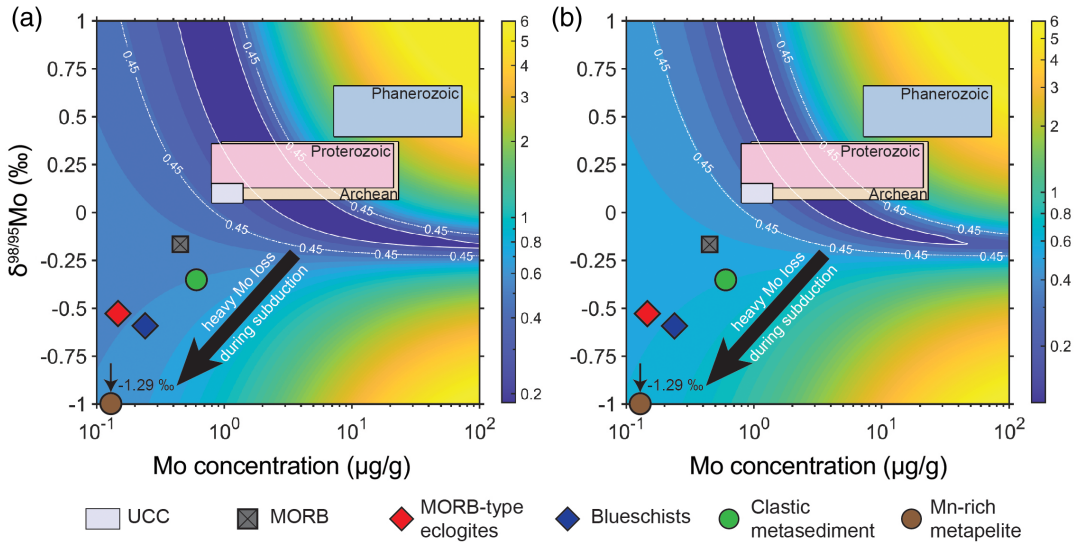

Figure 2 Least squares error ($\Delta^{98/95}$Mo in ‰; up to 6 ‰) between calculated mixing lines and analysed samples. Variables are the $\delta^{98/95}$Mo and [Mo] values derived from **(a)** the $\delta^{98/95}$Mo *vs.* $^{87}Sr/^{86}Sr$ and **(b)** the $\delta^{98/95}$Mo *vs.* $^{143}Nd/^{144}Nd$ relationship (Fig. 1). Literature values for potential (concentration averaged) recycled lithologies, and anoxic sediments sorted by age intervals are shown for comparison. See Table S-2 and Supplementary Information S-5 for references, mixing parameters, and further details.

subducted sedimentary Mo signature, which provides a context of deep ocean redox conditions.

Implications for the sedimentary Mo subduction cycle. Due to the anoxic conditions in the Proterozoic deep ocean, oxidised species of major and minor elements like Fe, S and Mn, were absent in deep sea sediments, thus lowering their redox budget/oxidising capacity compared to present day marine lithologies (*e.g.*, Evans, 2012; Ague *et al.*, 2022). This may also explain the preserved $\delta^{98/95}$Mo of a reduced Proterozoic sediment component recycled into the S-MAR mantle source, in contrast to Neoproterozoic, deep mantle recycling of low $\delta^{98/95}$Mo into mantle plume sources (see also Ma *et al.*, 2022). This is in line with Samoan OIBs, where $\delta^{98/95}$Mo signatures are interpreted as a mixture of isotopically heavy terrigenous sediments ($\delta^{98/95}$Mo ≈ UCC) and isotopically light dehydrated mafic oceanic crust, which reflect the influence of a distinct pool of mid-Proterozoic recycled ocean crust (Gaschnig *et al.*, 2021). Altogether, this indicates that changing Earth surface redox conditions have influenced the fO_2 conditions during subduction and the mobility of sedimentary Mo (and by analogy that of other redox sensitive elements) and hence, the Mo isotope budget between different Earth (silicate) reservoirs. This emphasises the time- and condition-related variations in Mo mobility during subduction on our planet (Fig. 3). We therefore conclude that the Mo isotope signature of plume-influenced volcanic rocks can be used to reconcile the redox conditions during

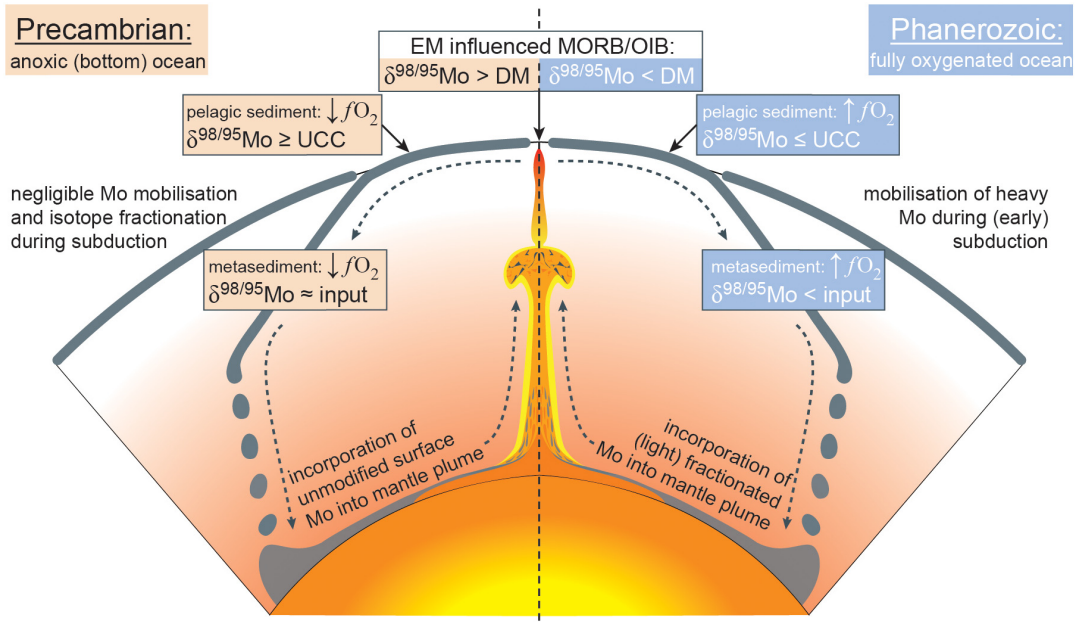

Figure 3 Illustration of the subducted sedimentary Mo cycle during the Precambrian (left) and Phanerozoic (right). Deep sea sediments carry variable redox budgets influencing Mo mobility and hence isotope fractionation during subduction over Earth's history (see text). UCC, upper continental crust; DM, depleted mantle; EM, enriched mantle.

ancient surface deposition of deep sea sediments (*cf.* Gaschnig *et al.*, 2021) as well as during subduction-related prograde metamorphism and the inception of modern subduction.

Acknowledgements

This work was funded by the Swiss National Science Foundation, Switzerland (Grant number 182508) to MW. The MC-ICP-MS at the Institute of Geological Sciences, University of Bern used in this study was acquired within the framework of the NCCR project PlanetS (Grant nr. 1NF40-141881) funded by the Swiss National Science Foundation. SK and CR acknowledge ERC Starting Grant 636808 (project O_2RIGIN). SK also acknowledges Ramón y Cajal contract RYC2020-030014-I. Jörg Hermann and Paolo Sossi are acknowledged for discussions that contributed to this manuscript. We also wish to thank Alex McCoy-West and two anonymous reviewers for constructive reviews, as well as Helen Williams for editorial handling.

Editor: Helen Williams

Additional Information

Supplementary Information accompanies this letter at https://www.geochemicalperspectivesletters.org/article2236.

Cite this letter as: Ahmad, Q., Wille, M., Rosca, C., Labidi, J., Schmid, T., Mezger, K., König, S. (2022) Molybdenum isotopes in plume-influenced MORBs reveal recycling of ancient anoxic sediments. *Geochem. Persp. Let.* 23, 43–48. https://doi.org/10.7185/geochemlet.2236

References

Ague, J.J., Tassara, S., Holycross, M.E., Li, J.-L., Cottrell, E., Schwarzenbach, E.M., Fassoulas, C., John, T. (2022) Slab-derived devolatilization fluids oxidized by subducted metasedimentary rocks. *Nature Geoscience* 15, 320–326. https://doi.org/10.1038/s41561-022-00904-7

Ahmad, Q., Wille, M., König, S., Rosca, C., Hensel, A., Pettke, T., Hermann, J. (2021) The Molybdenum isotope subduction recycling conundrum: A case study from the Tongan subduction zone, Western Alps and Alpine Corsica. *Chemical Geology* 576, 120231. https://doi.org/10.1016/j.chemgeo.2021.120231

Andres, M., Blichert-Toft, J., Schilling, J.-G. (2002) Hafnium isotopes in basalts from the southern Mid-Atlantic Ridge from 40°S to 55°S: Discovery and Shona plume–ridge interactions and the role of recycled sediments. *Geochemistry, Geophysics, Geosystems* 3, 1–25. https://doi.org/10.1029/2002GC000324

Bali, E., Keppler, H., Audetat, A. (2012) The mobility of W and Mo in subduction zone fluids and the Mo–W–Th–U systematics of island arc magmas. *Earth and Planetary Science Letters* 351–352, 195–207. https://doi.org/10.1016/j.epsl.2012.07.032

Burdige, D.J. (2007) Preservation of Organic Matter in Marine Sediments: Controls, Mechanisms, and an Imbalance in Sediment Organic Carbon Budgets? *Chemical Reviews* 107, 467–485. https://doi.org/10.1021/cr050347q

Chen, S., Hin, R.C., John, T., Brooker, R., Bryan, B., Niu, Y., Elliott, T. (2019) Molybdenum systematics of subducted crust record reactive fluid flow from underlying slab serpentine dehydration. *Nature Communications* 10, 4773. https://doi.org/10.1038/s41467-019-12696-3

Chen, S., Sun, P., Niu, Y., Guo, P., Elliott, T., Hin, R.C. (2022) Molybdenum isotope systematics of lavas from the East Pacific Rise: Constraints on the source of enriched mid-ocean ridge basalt. *Earth and Planetary Science Letters* 578, 117283. https://doi.org/10.1016/j.epsl.2021.117283

Chowdhury, P., Dasgupta, R., Phelps, P.R., Costin, G., Lee, C.-T. A. (2022) Oxygen fugacity range of subducting crust inferred from fractionation of trace elements during fluid-present slab melting in the presence of anhydrite versus sulfide. *Geochimica et Cosmochimica Acta* 325, 214–231. https://doi.org/10.1016/j.gca.2022.02.030

Douglass, J., Schilling, J.-G., Fontignie, D. (1999) Plume-ridge interactions of the Discovery and Shona mantle plumes with the southern Mid-Atlantic Ridge (40°-55°S). *Journal of Geophysical Research: Solid Earth* 104, 2941–2962. https://doi.org/10.1029/98JB02642

Evans, K.A. (2012) The redox budget of subduction zones. *Earth-Science Reviews* 113, 11–32. https://doi.org/10.1016/j.earscirev.2012.03.003

Freymuth, H., Vils, F., Willbold, M., Taylor, R.N., Elliott, T. (2015) Molybdenum mobility and isotopic fractionation during subduction at the Mariana arc. *Earth and Planetary Science Letters* 432, 176–186. https://doi.org/10.1016/j.epsl.2015.10.006

Freymuth, H., Elliott, T., van Soest, M., Skora, S. (2016) Tracing subducted black shales in the Lesser Antilles arc using molybdenum isotope ratios. *Geology* 44, 987–990. https://doi.org/10.1130/G38344.1

Gaschnig, R.M., Reinhard, C.T., Planavsky, N.J., Wang, X., Asael, D., Chauvel, C. (2017) The Molybdenum Isotope System as a Tracer of Slab Input in Subduction Zones: An Example From Martinique, Lesser Antilles Arc. *Geochemistry, Geophysics, Geosystems* 18, 4674–4689. https://doi.org/10.1002/2017GC007085

Gaschnig, R.M., Reinhard, C.T., Planavsky, N.J., Wang, X., Asael, D., Jackson, M.G. (2021) The impact of primary processes and secondary alteration on the stable isotope composition of ocean island basalts. *Chemical Geology* 581, 120416. https://doi.org/10.1016/j.chemgeo.2021.120416

Kendall, B., Dahl, T.W., Anbar, A.D. (2017) The stable isotope geochemistry of molybdenum. *Reviews in Mineralogy and Geochemistry* 82, 683–732. https://doi.org/10.2138/rmg.2017.82.16

König, S., Wille, M., Voegelin, A., Schoenberg, R. (2016) Molybdenum isotope systematics in subduction zones. *Earth and Planetary Science Letters* 447, 95–102. https://doi.org/10.1016/j.epsl.2016.04.033

Laakso, T.A., Schrag, D.P. (2019) A small marine biosphere in the Proterozoic. *Geobiology* 17, 161–171. https://doi.org/10.1111/gbi.12323

Labidi, J., Cartigny, P., Moreira, M. (2013) Non-chondritic sulphur isotope composition of the terrestrial mantle. *Nature* 501, 208–211. https://doi.org/10.1038/nature12490

le Roux, P., le Roex, A., Schilling, J.G. (2002a) MORB melting processes beneath the southern Mid-Atlantic Ridge (40–55°S): a role for mantle plume-derived pyroxenite. *Contributions to Mineralogy and Petrology* 144, 206–229. https://doi.org/10.1007/s00410-002-0376-3

le Roux, P.J., le Roex, A.P., Schilling, J.G., Shimizu, N., Perkins, W.W., Pearce, N.J.G. (2002b) Mantle heterogeneity beneath the southern Mid-Atlantic Ridge: trace element evidence for contamination of ambient asthenospheric mantle. *Earth and Planetary Science Letters* 203, 479–498. https://doi.org/10.1016/S0012-821X(02)00832-4

Lyons, T.W., Reinhard, C.T., Planavsky, N.J. (2014) The rise of oxygen in Earth's early ocean and atmosphere. *Nature* 506, 307–315. https://doi.org/10.1038/nature13068

Ma, L., Xu, Y.G., Li, J., Chen, L.-H., Liu, J.-Q., Li, H.-Y., Huang, X.-L., Ma, Q., Hong, L.-B., Wang, Y. (2022) Molybdenum isotopic constraints on the origin of EM1-type continental intraplate basalts. *Geochimica et Cosmochimica Acta* 317, 255–268. https://doi.org/10.1016/j.gca.2021.11.013

McCoy-West, A.J., Chowdhury, P., Burton, K.W., Sossi, P., Nowell, G.M., Fitton, J.G., Kerr, A.C., Cawood, P.A., Williams, H.M. (2019) Extensive crustal extraction in Earth's early history inferred from molybdenum isotopes. *Nature Geoscience* 12, 946–951. https://doi.org/10.1038/s41561-019-0451-2

Poulton, S.W., Canfield, D.E. (2011) Ferruginous Conditions: A Dominant Feature of the Ocean through Earth's History. *Elements* 7, 107–112. https://doi.org/10.2113/GSELEMENTS.7.2.107

Skora, S., Freymuth, H., Blundy, J., Elliott, T., Guillong, M. (2017) An experimental study of the behaviour of cerium/molybdenum ratios during subduction: Implications for tracing the slab component in the Lesser Antilles and Mariana Arc. *Geochimica et Cosmochimica Acta* 212, 133–155. https://doi.org/10.1016/j.gca.2017.05.025

Stolper, D.A., Keller, C.B. (2018) A record of deep-ocean dissolved O_2 from the oxidation state of iron in submarine basalts. *Nature* 553, 323–327. https://doi.org/10.1038/nature25009

Willbold, M., Elliott, T. (2017) Molybdenum isotope variations in magmatic rocks. *Chemical Geology* 449, 253–268. https://doi.org/10.1016/j.chemgeo.2016.12.011

Ye, Y., Zhang, S., Wang, H., Wang, X., Tan, C., Li, M., Wu, C., Canfield, D.E. (2021) Black shale Mo isotope record reveals dynamic ocean redox during the Mesoproterozoic Era. *Geochemical Perspectives Letters* 18, 16–21. https://doi.org/10.7185/geochemlet.2118

Yierpan, A., König, S., Labidi, J., Schoenberg, R. (2020) Recycled selenium in hot spot–influenced lavas records ocean-atmosphere oxygenation. *Science Advances* 6, abb6179. https://doi.org/10.1126/sciadv.abb6179

Geochemical Perspectives Letters

Molybdenum isotopes in plume-influenced MORBs reveal recycling of ancient anoxic sediments

Q. Ahmad, M. Wille, C. Rosca, J. Labidi, T. Schmid, K. Mezger, S. König

Supplementary Information

The Supplementary Information includes:

- Section S-1: Geochemical Background of the Samples
- Section S-2: Potential Controls on the Mo Isotope Variability of S-MAR Basalts
- Section S-3: Origin of Enriched Mantle
- Section S-4: Analytical Methods
- Section S-5: Misfit Model
- Supplementary Information References

Section S-1: Geochemical Background of the Samples

The studied samples are fresh basaltic glasses that were dredged from the South-Mid Atlantic Ridge (S-MAR) during the RV *Maurice Ewing* cruise EW93-09 (Douglass *et al.*, 1995, 1999). All samples were well-characterised in terms of radiogenic isotopes (Sr, Nd, Hf, and Pb) (Douglass *et al.*, 1999; Andres *et al.*, 2002), S isotopes (Labidi *et al.*, 2013), Se isotopes (Yierpan *et al.*, 2020), noble gases (Moreira *et al.*, 1995; Sarda *et al.*, 2000), and major and trace element abundances (le Roux *et al.*, 2002a, 2002b, 2002c; Kelley *et al.*, 2013). This makes the selected sample suite ideal for investigating their Mo isotope signature.

The most prominent feature in the S-MAR is the localised interaction between the ambient asthenospheric mantle and the Discovery and Shona mantle plumes (Fig. S-1). A variety of recycled components have been suggested to be incorporated in these mantle plumes based on radiogenic and stable isotope systematics (Fig. S-2; see references above).

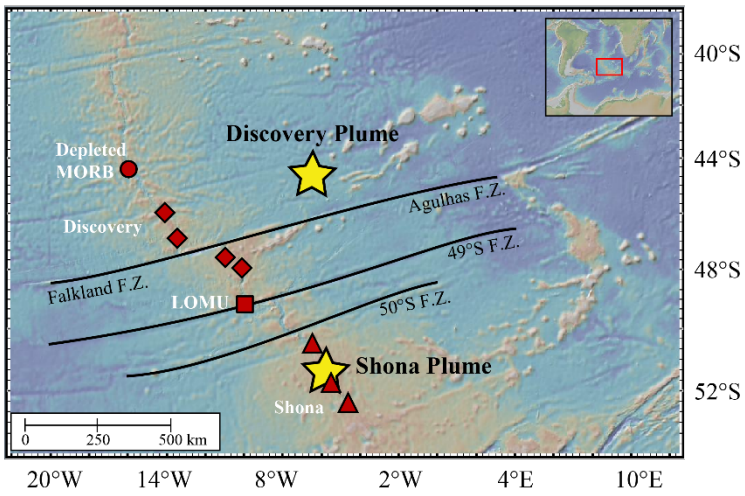

Figure S-1 Sample locations along the S-MAR together with the Discovery and Shona plume, as well as tectonic fracture zones (F.Z.). Figure made with GeoMapApp (www.geomapapp.org).

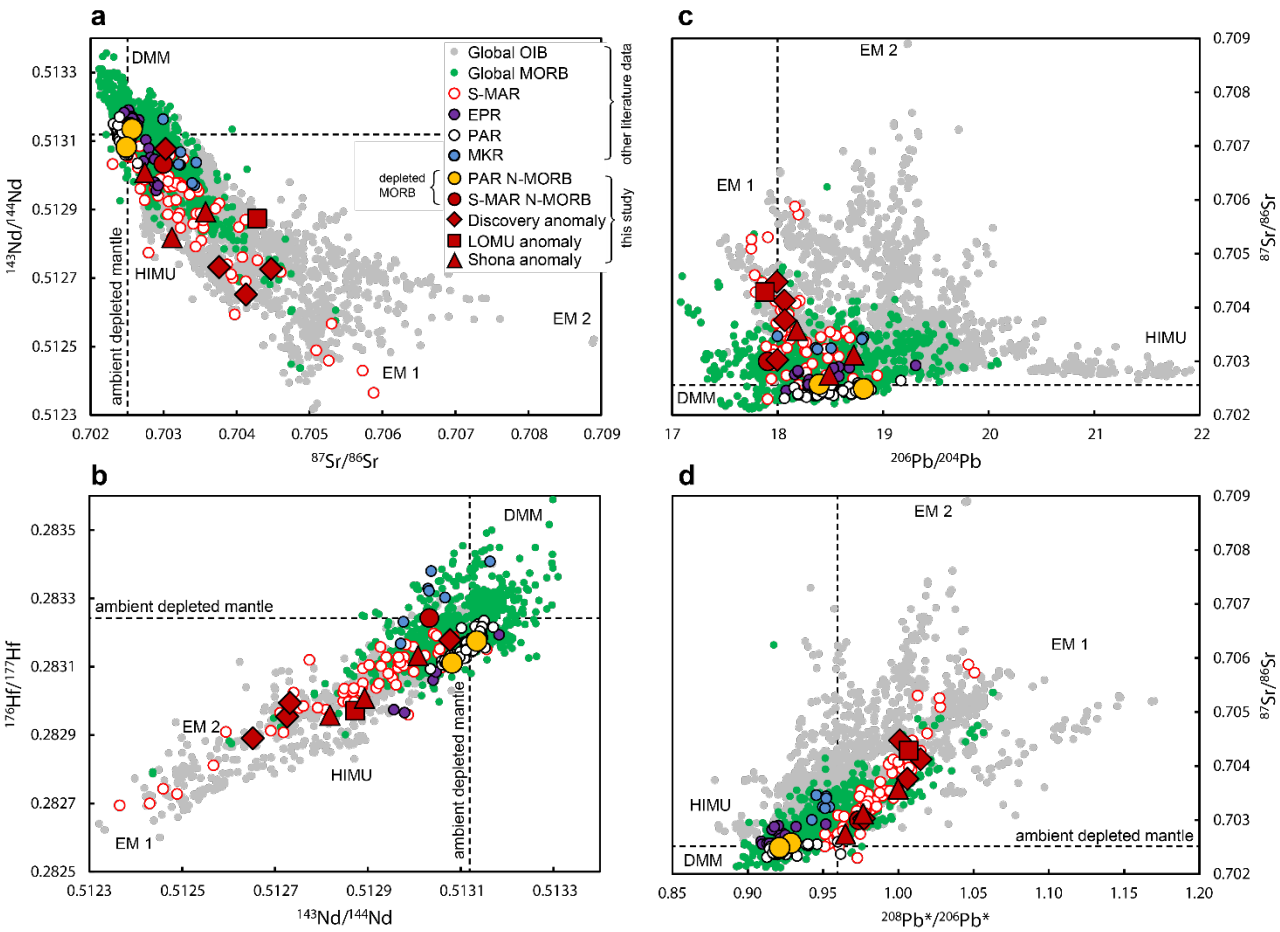

Figure S-2 Radiogenic isotope data for the studied S-MAR and PAR glasses, modified after Yierpan *et al.* (2020). Shown for comparison are a global compilation of MORB and OIB (Stracke, 2012 and references therein). MORBs (and seamounts) near the East Pacific Rise (EPR) (Chen *et al.*, 2022 and references therein), Mohns-Knipovich ridges (MKR) (Bezard *et al.*, 2016), and PAR (Hamelin *et al.*, 2011 and references therein) are plotted for comparision. A more detailed precompilation of S-MAR basalts can be found in Labidi *et al.* (2013). Dashed lines indicate the composition of the S-MAR ambient depleted mantle (Douglass *et al.*, 1999; Andres *et al.*, 2002). In **(d)**, $^{208}Pb^*/^{206}Pb^*$ exemplifies the time-integrated Th/U ratios (Stracke, 2012).

Two additional samples from the Pacific-Antarctic Ridge (PAR) complement existing PAR-MORB Mo isotope data (Bezard *et al.*, 2016). This setting is dominantly sourced by depleted mantle being devoid of any deep mantle plume influence (*e.g.*, Hamelin *et al.*, 2011) with radiogenic Sr and Nd isotope signature similar to the ambient depleted mantle (ADM) constrained for the S-MAR suite (Table S-2; Douglass *et al.*, 1999; Andres *et al.*, 2002).

Section S-2: Potential Controls on the Mo Isotope Variability of S-MAR Basalts

Observed correlations between $\delta^{98/95}$Mo and ^{143}Nd/^{144}Nd or ^{176}Hf/^{177}Hf (Figs. 1, S-4a) exclude post-emplacement seawater alteration effects on the Mo isotope composition, as seawater incorporation is insensitive to relatively fluid-immobile Nd or Hf (see Labidi *et al.*, 2013). This is also supported by Cl/K ratios close to the range of global MORB (Table S-1) (Labidi *et al.*, 2013). Also unlikely is isotope fractionation due to segregation of an isotopically heavy sulfide melt at low melting degrees, which results into an isotopically light silicate melt (Liang *et al.*, 2017). The studied samples were sulfide-saturated during melting (Labidi *et al.*, 2013 and references therein), however, there is no correlation between $\delta^{98/95}$Mo and Mo/Ce, with Ce being similarly incompatible during mantle melting but Mo being more compatible in presence of a segregated sulfide melt. Furthermore, a potential sulfide melt segregation would have removed any relationship between $\delta^{98/95}$Mo, and radiogenic isotopes (see Labidi *et al.*, 2013). This covariation together with lack of covariations between $\delta^{98/95}$Mo and MgO or Mg#, and overall high MgO contents (Table S-1) suggests that also fractional crystallisation during differentiation is not the cause of the observed Mo isotope variation (*e.g.*, Voegelin *et al.*, 2014). This is in line with other tholeiitic systems (*e.g.*, Yang *et al.*, 2015; Bezard *et al.*, 2016).

Elemental systematics of S-MAR basalts suggest mixing of ambient mantle with low-degree melts (F = 2–3 %; le Roux *et al.*, 2002b). Previously, elevated $\delta^{98/95}$Mo in lavas from the EPR (devoid of a mantle plume component) were interpreted to reflect mixing of depleted MORB with an isotopically heavy end member of magmatic origin without contribution of recycled crustal components (Chen *et al.*, 2022). The authors argued that this heavy end member is an ancient (>1 Ga) low-degree melt (F = 0.2 %) of depleted mantle material that led to an initial fractionation of $\delta^{98/95}$Mo (due to different magmatic compatibilities of Mo^{4+} and Mo^{6+}; McCoy-West *et al.*, 2019), similar incompatible elements (*e.g.*, Nb/Zr), and further parent-daughter ratios of radiogenic isotopes. This explains the observed correlation of $\delta^{98/95}$Mo and radiogenic isotopes of Pb, Nd, and Sr (Chen *et al.*, 2022). In the S-MAR sample suite, the trace element ratios are accompanied by radiogenic isotope systematics attributable to an enriched mantle 1 (EM1) signature requiring a higher initial Rb/Sr, lower Sm/Nd and Lu/Hf, and similar U/Pb compared to DMM (Fig. S-2). These signatures, however, are primary and cannot be explained by low-F melting of plume mantle material (le Roux *et al.*, 2002b). Furthermore, plume-material is pre-enriched in isotopically heavy S and Se prior to low-F

melting (Labidi *et al.*, 2013; Yierpan *et al.*, 2020). The question remains, if heavy Mo is primary or if it is generated during low-*F* mantle melting. If we consider a low-*F* melting of *F* = 2.5 % melting (le Roux *et al.*, 2002b) of plume material (*T* = 1200 °C; $Mo^{6+}/\Sigma Mo$ = 0.99), we would expect a maximum isotope shift of $\Delta^{98/95}Mo_{max}$ of ~ 0.085 ‰ between pyroxenite melt and DMM (*F* = 15 %) (McCoy-West *et al.*, 2019). A mixture of both of these end members with 20 % pyroxenite contribution in our heaviest sample EW9309 33D-1g (le Roux *et al.*, 2002b) would lead to a maximum $\Delta^{98/95}Mo_{max}$ of 0.059 ‰ (melting model from Wang and Becker, 2018). This value is likely lower ($\Delta^{98/95}Mo_{max}$ = 0.040 ‰) when considering lower N-MORB like [Mo] of pyroxenite melts, as there is no covariation of $\delta^{98/95}$Mo and Mo/Ce (Fig. S-5). Moreover, these pyroxenites are formed along the plume-adiabat, which is hotter than the N-MORB adiabat, lowering further the isotopic fractionation induced by low-*F* melting. Furthermore, we do not observe a correlation of $\delta^{98/95}$Mo with Pb isotopes, which is inconsistent with the increase of U/Pb during ancient low-*F* melting (Chen *et al.*, 2022). In contrast, we observe LOMU-samples that carry an isotopic heavy signature, which is consistent with an *e.g.*, Proterozoic sediment contribution (*e.g.*, Rehkämper and Hofmann, 1997; Douglass *et al.*, 1999; Andres *et al.*, 2002). As correlations between radiogenic isotopes and $\delta^{34/32}$S, $\delta^{82/76}$Se, and $\delta^{98/95}$Mo (*e.g.*, Fig. 1, S-4b) cannot be explained by magmatic processes or post-emplacement alteration (see Labidi *et al.*, 2013; Yierpan *et al.*, 2019, 2020, 2021), this relationship is in strong support of recycling of enriched mantle components with $\delta^{98/95}$Mo > depleted mantle.

Table S-1 Average and individual Mo isotope and elemental data of analysed MORBs from S-MAR and PAR. MgO and calculated Cl/K are from (le Roux *et al.*, 2002a; Labidi *et al.*, 2013). Individual measurements represent separate sample digestions and chromatographic separations. *Internal precision on a sample run (over 80 cycles) is reported as 2 standard error (2 s.e.).

Sample	Type	Individual measurements			Mean values				
		$\delta^{98/95}$Mo (‰)	2 s.e.* (‰)	Mo (µg/g)	$\delta^{98/95}$Mo (‰)	2 s.d. (‰)	Mo (µg/g)	MgO (wt. %)	Cl/K
	Southern Mid-Atlantic ridge								
EW9309 40D-1g	Depleted N-MORB	−0.226 −0.201 −0.265	0.015 0.022 0.020	0.254 0.255 0.254	−0.231	0.064	0.254	8.30	0.11
EW9309 33D-1g	Discovery influenced MORB (North)	−0.100 −0.073 −0.121	0.013 0.020 0.013	1.25 1.25 1.25	−0.098	0.048	1.25	7.83	0.04
EW9309 28D-1g	Discovery influenced MORB (North)	−0.191 −0.287	0.018 0.018	0.168 0.170	−0.239	0.136	0.169	8.22	0.06
EW9309 2D-1g	Discovery influenced MORB (South)	−0.122 −0.174	0.020 0.014	0.665 0.661	−0.148	0.074	0.663	6.24	0.03
EW9309 4D-3g	Discovery influenced MORB (South)	−0.136 −0.124 −0.195	0.015 0.020 0.016	0.539 0.527 0.517	−0.152	0.077	0.528	7.60	0.04
EW9309 9D-3g	LOMU MORB	−0.167 −0.199	0.017 0.015	0.654 0.654	−0.183	0.045	0.654	8.67	0.06
EW9309 15D-1g	Shona influenced MORB	−0.199 −0.215	0.028 0.019	0.363 0.364	−0.207	0.023	0.364	7.81	0.08
EW9309 21D-1g	Shona influenced MORB	−0.179 −0.196	0.027 0.013	0.587 0.585	−0.188	0.024	0.586	7.10	0.05
EW9309 22D-3g	Shona influenced MORB	−0.155 −0.219	0.019 0.017	1.03 1.03	−0.187	0.090	1.03	4.83	0.07

Table S-1 continued.

Sample	Type	Individual measurements			Mean values				
		$\delta^{98/95}$Mo (‰)	2 s.e.* (‰)	Mo (µg/g)	$\delta^{98/95}$Mo (‰)	2 s.d. (‰)	Mo (µg/g)	MgO (wt. %)	Cl/K
	Pacific-Antarctic ridge								
PAC2 DR33-1	Depleted N-MORB	−0.225	0.018	0.470	−0.245	0.062	0.462	6.63	-
		−0.228	0.028	0.461					
		−0.281	0.016	0.454					
PAC1 CV-02g	Depleted N-MORB	−0.249	0.016	0.213	−0.297	0.116	0.215	7.74	-
		−0.280	0.031	0.213					
		−0.361	0.021	0.218					
	Rock reference materials								
AGV-2	Andesite	−0.192	0.015	2.13	−0.194	0.042	2.14	-	-
		−0.211	0.019	2.11					
		−0.179	0.012	2.19					
BHVO-2	Basalt	−0.092	0.015	3.43	−0.108	0.032	3.68	-	-
		−0.099	0.017	4.64					
		−0.132	0.015	2.96					
W-2a	Diabase	−0.100	0.018	0.462	−0.087	0.053	0.452	-	-
		−0.104	0.021	0.455					
		−0.057	0.010	0.439					

Section S-3: Origin of Enriched Mantle

Different recycled components (*e.g.*, sub-continental mantle, lower continental crust, oceanic crust, and sediment) in the mantle source of the S-MAR (Douglass *et al.*, 1999; Andres *et al.*, 2002; le Roux *et al.*, 2002c; Labidi *et al.*, 2013; Yierpan *et al.*, 2020) can have an influence on $\delta^{98/95}$Mo of the samples. Sub-continental mantle can be excluded as a significant component, since worldwide peridotites have a MORB-like $\delta^{98/95}$Mo (–0.206 ± 0.05 ‰; Liang *et al.*, 2017). An aqueous fluid expelled from subducted crust can influence the mantle composition leading to elevated $\delta^{98/95}$Mo and [Mo] (*e.g.*, Ahmad *et al.*, 2021); however, we observe correlations between $\delta^{98/95}$Mo and aqueous fluid-immobile Nd and Hf isotopes (Figs. 1, S-4a) and no covariation is observed with fluid proxies, such as Ba/Th ($R^2 = 0.1$). There is no direct estimate of $\delta^{98/95}$Mo of the lower continental crust (LCC), however, cumulates which possibly reside in the LCC, likely incorporate preferentially light Mo isotopes (Wille *et al.*, 2018; Nebel-Jacobsen *et al.*, 2021) and are unsuitable candidates to explain Mo signatures in the basalt samples. Apart from a clear EM1 affinity, two samples analysed here show a trend towards HIMU (Fig. S-2), thus a signature of recycled AOC. However, ^{206}Pb/^{204}Pb ratios do not correlate with $\delta^{98/95}$Mo and most radiogenic ^{206}Pb/^{204}Pb values are accompanied with depleted mantle-like $\delta^{98/95}$Mo (Fig. S-4c). This leads to the conclusion that a significant influence of recycled AOC is unlikely. Furthermore, prograde subduction metamorphism can modify the AOC Mo isotopic signature to lighter values than mantle due to AOC and serpentinite dehydration (Freymuth *et al.*, 2015; Chen *et al.*, 2019), which is also not observed. Oxic sediments are no suitable candidates, as a) oxidised Phanerozoic subducted metasediments are characterised by $\delta^{98/95}$Mo lower than mantle (Ahmad *et al.*, 2021) and b) modelled Mid-Proterozoic sediment recycling ages (Douglass *et al.*, 1999; Andres *et al.*, 2002; Labidi *et al.*, 2013) suggest anoxic deep ocean redox conditions during the Proterozoic (*e.g.*, Lyons *et al.*, 2014). Based on previous stable S and Se studies, the recycled sediment component is likely anoxic and experienced negligible subduction-related S and Se mobilisation (Labidi *et al.*, 2013; Yierpan *et al.*, 2020) indicating a stable sedimentary sulfide phase (and potential Mo host) during potential hotter subduction zone conditions in the Proterozoic. This is in line with a previous Mo isotope study on a partially melted Archean eclogite, which indicates stable Mo host phases such as rutile and sulfide (Greaney *et al.*, 2018). Preservation of isotopically heavy Se and Mo in the recycled component further indicates that there was negligible modification by oxidising fluids during anoxic Proterozoic sediment subduction (see König *et al.*, 2021; see discussion in the main text). In line with previous investigations showing covariations between fO_2-sensitive stable Se-S isotope systematics and radiogenic isotopes, $\delta^{98/95}$Mo higher than depleted mantle, and overall low Mo mobility during anoxic sediment subduction (see discussion in the main text) we suggest that an anoxic Proterozoic sediment contribution to the S-MAR mantle source is the most likely scenario for the observed heavy Mo isotope enrichment in our samples.

Section S-4: Analytical Methods

Molybdenum purification and isotope analysis was conducted in the clean laboratory facilities at the Institute of Geological Sciences, University of Bern. For all samples, enough powder was weighed to have 25–50 ng Mo for analysis. The material was spiked with an enriched isotope tracer solution (^{97}Mo-^{100}Mo double spike). The samples were then dissolved in concentrated single distilled acids in the following sequence: (*i*) concentrated HF-HNO_3 (3:1 mixture), (*ii*) concentrated HNO_3, (*iii*) 6 M HCl in Savillex™ Teflon vials. The dissolved samples were processed through anion- and cation exchange columns to obtain a clean Mo separate (Wille *et al.*, 2013). In the first step, samples were taken up in 4 M HCl and passed through Dowex 1X8, 200–400 mesh, anion resin. In a second step, the sample material was taken up in 0.5 M HCl and passed through Dowex 50WX8 200–400 mesh, cation exchange resin. Stable Mo isotope measurements were carried out on a Neptune Plus MC-ICPMS coupled with an Aridus II desolvating nebuliser with an uptake rate of 100–150 µL min^{-1} (details are provided in Ahmad *et al.*, 2021). Six Mo isotopes (^{94}Mo, ^{95}Mo, ^{96}Mo, ^{97}Mo, ^{98}Mo and ^{100}Mo) were measured as well as ^{99}Ru and ^{101}Ru to monitor potential isobaric interference. We used resistors with 10^{-11} Ω to analyse all isotopes except ^{101}Ru, which was measured using a 10^{-12} Ω resistor. For analyses, we have used a combination of 'H' Ni sampler cone and 'X' Ni skimmer cone and obtained ~120 V/ppm on ^{95}Mo. We used a double spike correction method based on an iterative calculation procedure (see Siebert *et al.*, 2001). The total procedural blank was between 0.22 to 0.65 ng. We present all data in the δ notation and relative to NIST SRM 3134 in ‰ (Greber *et al.*, 2012; Goldberg *et al.*, 2013) with an interference correction based on ^{99}Ru:

$$\delta^{98/95}\mathrm{Mo} = \left(\frac{\left(\frac{^{98}\mathrm{Mo}}{^{95}\mathrm{Mo}}\right)_{\mathrm{Sample}}}{\left(\frac{^{98}\mathrm{Mo}}{^{95}\mathrm{Mo}}\right)_{\mathrm{NIST\ SRM\ 3134}}} - 1 \right) * 1{,}000 \qquad \text{(S-1)}$$

Interference-corrected $\delta^{98/95}$Mo ratios based on ^{99}Ru and ^{101}Ru correction were compared to ensure accurate determination of the Ru interference. Background correction was obtained by bracketing samples with measurements of 0.5 M HNO_3 carrier solution on-peak. Sample and background analysis consisted of 80 and 30 cycles, respectively, with a signal integration time of 4.194 s for each cycle. Repeated measurements of the standard NIST SRM 3134 and an in-house J&M standard solution lot 602332B gave an isotopic difference of $\Delta^{98/95}$Mo = 0.269 ± 0.017 ‰ (2 s.d., n = 14), in agreement with Greber *et al.* (2012) and Ahmad *et al.* (2021). Solution standards were measured at a concentration of 25 ppb. Individually digested and chemically purified whole-rock reference materials AGV-2, BHVO-2 and W-2a yielded a $\delta^{98/95}$Mo of −0.19 ± 0.03 ‰ (2 s.d., n = 3), −0.11 ± 0.04 ‰ (2 s.d., n = 3) and −0.09 ± 0.05 ‰ (2 s.d., n = 3), respectively (Table S-1). The

values are within uncertainty of those determined previously (*e.g.*, Burkhardt *et al.*, 2014; Willbold *et al.*, 2016; Zhao *et al.*, 2016). Individual measurements of whole rock reference materials (Table S-1) are within the long-term 2 s.d. external reproducibility of ±0.05 ‰ as determined by previous measurements of BHVO-2 (Ahmad *et al.*, 2021). Including these previous BHVO-2 measurements (−0.09 ± 0.05 ‰, n = 10), we consider ±0.05 ‰ as the long-term 2 s.d. external reproducibility of our sample measurements. All samples were measured multiple times (after individual digestions and chemical separation) and obtained $\delta^{98/95}$Mo and Mo concentration values were averaged for data presentation and interpretation (Table S-1). All individual sample measurements are within ±0.05 ‰ compared to their average $\delta^{98/95}$Mo, except PAR sample PAC CV-02g.

Section S-5: Misfit Model

The "linear" Mo-Sr(-Nd) isotope sample array (Fig. 1) represents only a small segment relative to the sediment end member (Table S-2), suggesting that a hyperbolic mixing curve could also account for the observed correlation. Mixing of two components (sediment, 'SED', and ambient depleted mantle end members, 'DM') with different Mo-Sr(-Nd) isotope compositions and concentrations will result in a hyperbola (*cf.* Vollmer, 1976) of the form:

$$Ax + Bxy + Cy + D = 0 \quad \text{(S-2)}$$

where

$$A = a_{\mathrm{DM}} b_{\mathrm{SED}} y_{\mathrm{DM}} - a_{\mathrm{SED}} b_{\mathrm{DM}} y_{\mathrm{SED}} \quad \text{(S-3)}$$
$$B = a_{\mathrm{SED}} b_{\mathrm{DM}} - a_{\mathrm{DM}} b_{\mathrm{SED}} \quad \text{(S-4)}$$
$$C = a_{\mathrm{DM}} b_{\mathrm{SED}} x_{\mathrm{SED}} - a_{\mathrm{SED}} b_{\mathrm{DM}} x_{\mathrm{DM}} \quad \text{(S-5)}$$
$$D = a_{\mathrm{SED}} b_{\mathrm{DM}} x_{\mathrm{DM}} y_{\mathrm{SED}} - a_{\mathrm{DM}} b_{\mathrm{SED}} x_{\mathrm{SED}} y_{\mathrm{DM}} \quad \text{(S-6)}$$

and

$x = {}^{87}\mathrm{Sr}/{}^{86}\mathrm{Sr}$ or ${}^{143}\mathrm{Nd}/{}^{144}\mathrm{Nd}$
$y = \delta^{98/95}\mathrm{Mo}$

$a_{\mathrm{SED}} = $ conc. of Mo
$b_{\mathrm{SED}} = $ conc. of ${}^{86}\mathrm{Sr}$ (~Sr) or ${}^{144}\mathrm{Nd}$ (~Nd)

} of the sediment end member with the isotopic composition $(x_{\mathrm{SED}}/y_{\mathrm{SED}})$

$a_{\mathrm{DM}} = $ conc. of Mo
$b_{\mathrm{DM}} = $ conc. of ${}^{86}\mathrm{Sr}$ (~Sr) or ${}^{144}\mathrm{Nd}$ (~Nd)

} of the depleted mantle end member with the isotopic composition $(x_{\mathrm{DM}}/y_{\mathrm{DM}})$.

By inserting Mo, Sr, and Nd concentrations and isotope compositions from the literature (Table S-2) into above equations, this leads to two unknowns of the sediment end member, a_{SED} and y_{SED}. By varying a_{SED}

from $a_{\mathrm{SED,\,min}}$ to $a_{\mathrm{SED,\,max}}$ and y_{SED} from $y_{\mathrm{SED,\,min}}$ to $y_{\mathrm{SED,\,max}}$, a total least squares error can be determined for each $\delta^{98/95}\mathrm{Mo}^{\mathrm{exp}}$ generated at a given $^{87}\mathrm{Sr}/^{86}\mathrm{Sr}$ or $^{143}\mathrm{Nd}/^{144}\mathrm{Nd}$ against the observed sample points as:

$$\sum_{i=a_{\mathrm{SED,\,min}}}^{a_{\mathrm{SED,\,max}}} \sum_{j=y_{\mathrm{SED,\,min}}}^{y_{\mathrm{SED,\,max}}} \sqrt{\left(\delta^{98/95}\mathrm{Mo}_{i,j}^{\mathrm{exp}} - \delta^{98/95}\mathrm{Mo}^{\mathrm{sample}}\right)^2} \quad \text{(S-7)}$$

where $a_{\mathrm{SED,\,min}}$ = 0.1 µg/g, $a_{\mathrm{SED,\,max}}$ = 100 µg/g, $y_{\mathrm{SED,\,min}}$ = −1 ‰, and $y_{\mathrm{SED,\,max}}$ = 1 ‰.

In the obtained misfit plot (Fig. 2), the best agreement between potential sediment end member and measured samples is given by the least squares error (blue banana) of the misfit function. The white dashed line indicates the sample amount multiplied by the external 2 s.d. reproducibility to obtain a conservative upper limit of model compositions. The white solid line indicates the contour line of the least squares error obtained (see minimum $\Delta^{98/95}$Mo in Fig. 2a, b) added by $\Delta^{98/95}\mathrm{Mo} \approx 0.1$ ‰. For comparison, the compositions of OM-rich sediments sorted by age intervals (Ye *et al.*, 2021; Table S-2), UCC (Greber *et al.*, 2014; Rudnick and Gao, 2014; Voegelin *et al.*, 2014; Freymuth *et al.*, 2015; Willbold and Elliott, 2017; Yang *et al.*, 2017; Greaney *et al.*, 2020;), MORB (Gale *et al.*, 2013; Bezard *et al.*, 2016; Chen *et al.*, 2022;), pelagic Mn-rich and clastic metasediments (Ahmad *et al.*, 2021), and blueschists and MORB-type eclogites (Chen *et al.*, 2019; Ahmad *et al.*, 2021) are plotted (Fig. 2).

Additional scenarios considered for misfit calculations, such as 1 Ga and 2 Ga model sediments, are plotted in Figure S-3 and show least squares errors similar to those in Figure 2. This indicates that a mid-Proterozoic UCC-like sediment with minor authigenic Mo enrichment is a likely sediment end member (see main text).

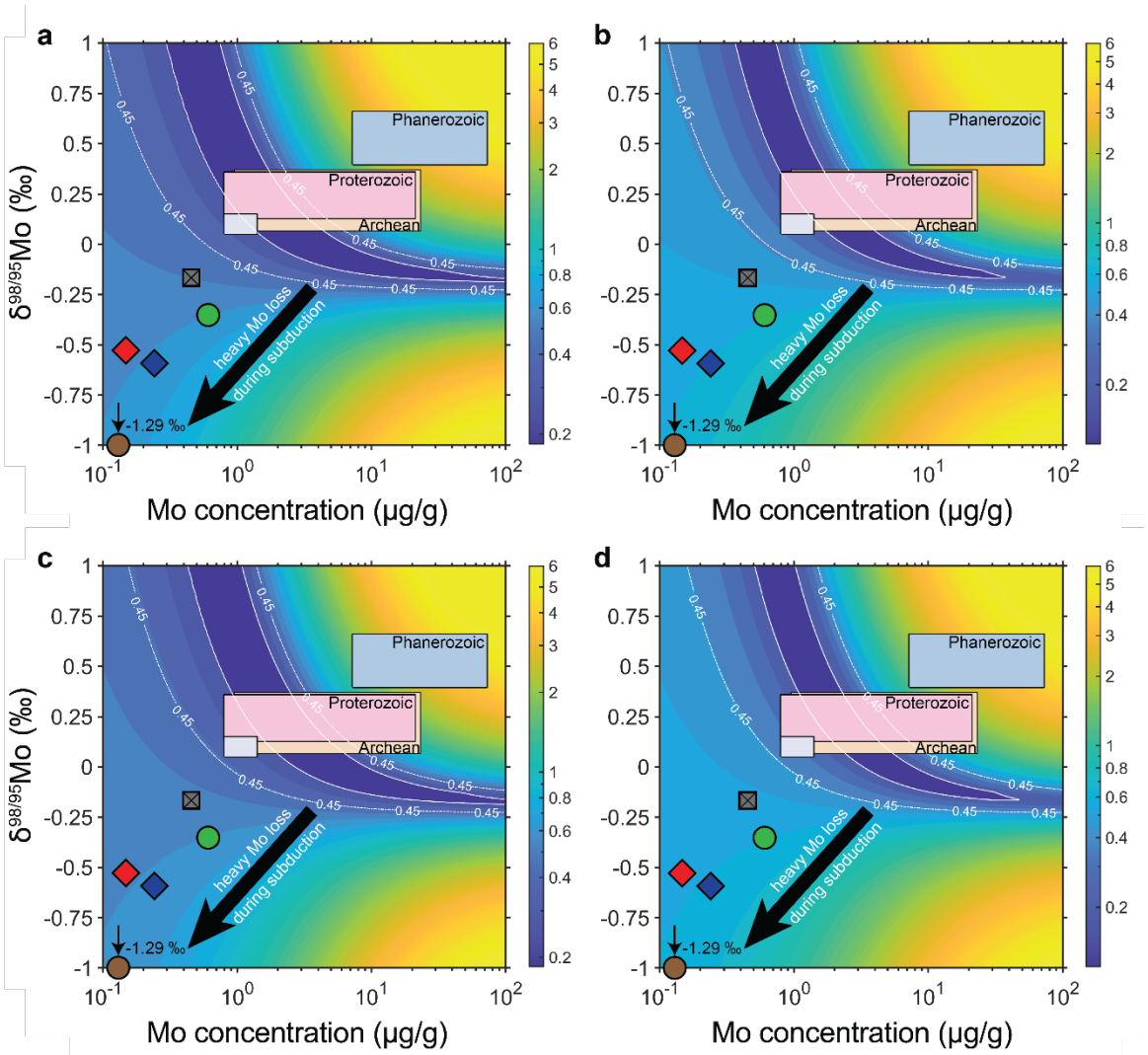

Figure S-3 Misfit calculation based on mixing parameters reported in Figure 2 and adjusted time-integrated Sr and Nd isotope compositions of the model sediment: **(a)** $^{87}Sr/^{86}Sr$ (1 Ga) = 0.7173; **(b)** $^{143}Nd/^{144}Nd$ (1 Ga) = 0.5115; **(c)** $^{87}Sr/^{86}Sr$ (2 Ga) = 0.7233; **(d)** $^{143}Nd/^{144}Nd$ (2 Ga) = 0.5119.

Table S-2 Parameters from the two-component mixing model (Fig. 2) and compositions of marine sediments.

	$\delta^{98/95}$Mo (‰)	[Mo] (µg/g)	$^{87}Sr/^{86}Sr$	Sr (µg/g)	$^{143}Nd/^{144}Nd$	Nd (µg/g)
End members						
Ambient depleted mantle	−0.245 ± 0.05[A]	0.025 ± 0.007	0.70250 or *0.702488 ± 0.000032*	9.80 ± 1.86	0.51312 or *0.513135 ± 0.00002*	0.713 ± 0.05
1.5 Ga old recycled pelagic sediment	0.78 ± 0.20[B] or *0.12 ± 0.06*[B]	0.76[B] or *2.98*[B]	0.7203	300 ± 17	0.5117	85 ± 5.2[C]
Marine sediments[D]						
Archean	0.218 ± 0.150 (*M* = 19, *N* = 417)	$4.70^{+18.4}_{-3.75}$ (*M* = 19, *N* = 744)				
Proterozoic	0.244 ± 0.114 (*M* = 51, *N* = 696)	$4.10^{+17.0}_{-3.30}$ (*M* = 53, *N* = 1262)				
Phanerozoic	0.528 ± 0.132 (*M* = 48, *N* = 882)	$22.9^{+49.7}_{-15.7}$ (*M* = 48, *N* = 1154)				

The mixing trends are generated using compositions of the Pacific/ambient depleted mantle or the most depleted MORB: PAC2 DR33-1 and PAC1 CV-02g (in italics). Uncertainties on mixing end member elemental concentrations (Rehkämper and Hofmann, 1997; Salters and Stracke, 2004; Labidi *et al.*, 2013; Plank, 2014; Yierpan *et al.*, 2020) and on [Mo]-$\delta^{98/95}$Mo values of the marine sediment compilation (Ye *et al.*, 2021) are all 1σ (except [Mo] uncertainty in depleted mantle, see Salters and Stracke, 2004).

Pelagic sediment and ambient mantle end member isotope compositions (Rehkämper and Hofmann, 1997; Andres *et al.*, 2002; le Roux *et al.*, 2002c; Labidi *et al.*, 2013; Yierpan *et al.*, 2020) are reported with 1σ uncertainties, (except $\delta^{98/95}$Mo uncertainty, which is reported as 2σ). *M* = number of age averaged data, *N* = number of different sediment samples from the literature.

[A] The Mo isotope composition of the Pacific-Antarctic Ridge (PAR) basalts can be used as the depleted mantle end member, because their Sr and Nd isotope composition match the S-MAR ambient depleted mantle isotopic composition determined previously (Douglass *et al.*, 1999; Andres *et al.*, 2002). The Mo isotope composition of the depleted N-MORB DR33-1g ($\delta^{98/95}$Mo = −0.245 ± 0.05 ‰) matches the light isotope composition of Phanerozoic Gorgona komatiites ($\delta^{98/95}$Mo = −0.18 to −0.25 ‰, McCoy-West *et al.*, 2019) and the lighter end of PAR basalts measured previously ($^{98/95}$Mo = −0.06 to −0.24 ‰, excluding the three heavy outliers; Bezard *et al.*, 2016). Because $\delta^{98/95}$Mo values of S-MAR basalts (and MORBs from EPR and PAR, Fig. 1) extend towards slightly lower values (but still within error) compared to the mean depleted mantle estimate (*e.g.*, McCoy-West *et al.*, 2019), we use this lower end of observed literature values for the ambient depleted mantle. The depleted N-MORB CV-02g ($\delta^{98/95}$Mo = −0.297 ± 0.05 ‰), however, represents an outlier being lighter than this range (but still within error) and is excluded in this model.

Table S-2 continued.

[B] Obtained best fit parameters from linear correlation between Mo-Sr isotope and Mo-Nd isotope (italic font) trend and the Mo, Sr, and Nd contents of depleted mantle and 1.5 Ga pelagic sediment (see above). Note the discrepancy between both $\delta^{98/95}$Mo and [Mo] obtained from both relationships (Fig. 1).

[C] Assigned relative error from GLOSS-II (Plank, 2014) as there was no uncertainty considered for pelagic sediment Nd content.

[D] Marine sediment values of different eons are log-normal means of sediments sorted by age intervals (>1 Myr) from the literature (see compilation of Ye *et al.*, 2021). The literature data represent mostly shallow-marine (continental shelf/closed basins) sediments from anoxic/euxinic settings, where *e.g.*, sulfate reduction leads to higher authigenic accumulation of isotopically heavy Mo from seawater compared to lower Mo accumulation in the anoxic deep sea (see main text).

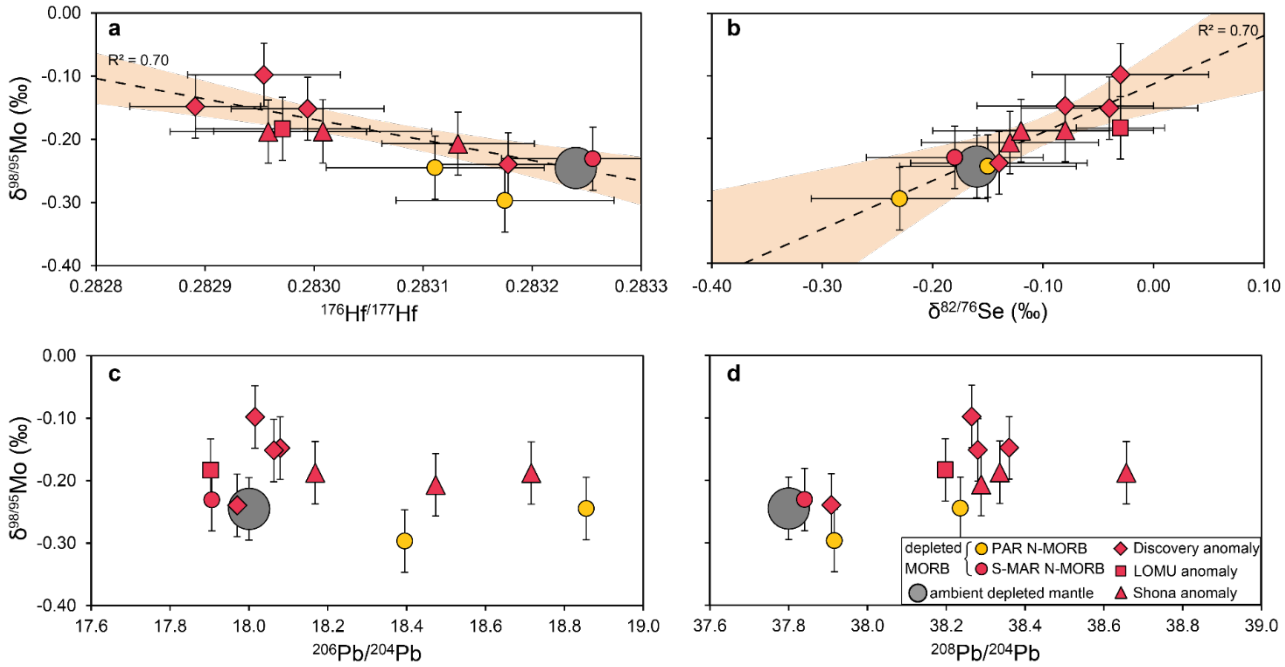

Figure S-4 Covariation diagram of S-MAR samples with: **(a)** $\delta^{98/95}$Mo *vs.* ^{176}Hf/^{177}Hf; **(b)** $\delta^{98/95}$Mo *vs.* δ^{82}Se **(c)** $\delta^{98/95}$Mo *vs.* ^{206}Pb/^{204}Pb; and **(d)** $\delta^{98/95}$Mo *vs.* ^{208}Pb/^{204}Pb. Error bars indicate 2 s.d. external reproducibility. External reproducibility on each isotope value is considered for regressions in **(a)** and **(b)**, and shaded areas indicate 95 % CI error envelope. PAR samples are excluded from the regression. Radiogenic isotopes and Se isotopes for this sample set together with ambient depleted mantle values are from Douglass *et al.* (1999), Andres *et al.* (2002), and Yierpan *et al.* (2020).

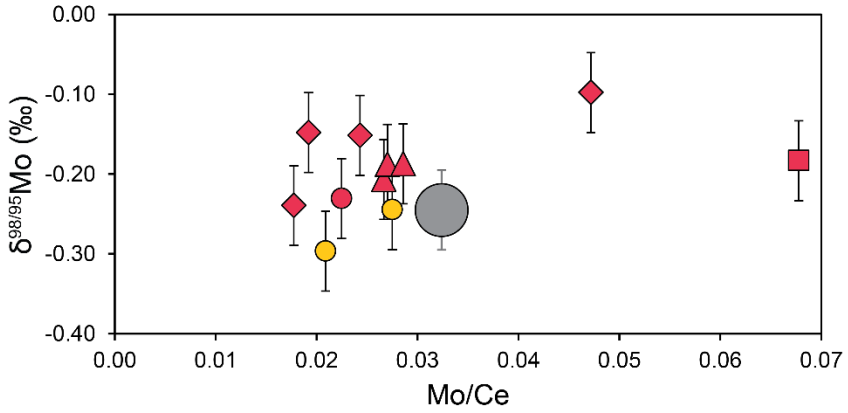

Figure S-5 Covariation diagram of S-MAR samples with $\delta^{98/95}$Mo *vs.* Mo/Ce. Ce contents of samples and depleted mantle Mo/Ce are from Salters and Stracke (2004) and Kelley *et al.* (2013).

Supplementary Information References

Ahmad, Q., Wille, M., König, S., Rosca, C., Hensel, A., Pettke, T., Hermann, J. (2021) The Molybdenum isotope subduction recycling conundrum: A case study from the Tongan subduction zone, Western Alps and Alpine Corsica. *Chemical Geology* 576, 120231. https://doi.org/10.1016/j.chemgeo.2021.120231

Andres, M., Blichert-Toft, J., Schilling, J.-G. (2002) Hafnium isotopes in basalts from the southern Mid-Atlantic Ridge from 40°S to 55°S: Discovery and Shona plume–ridge interactions and the role of recycled sediments. *Geochemistry*, *Geophysics*, *Geosystems* 3, 1–25. https://doi.org/10.1029/2002GC000324

Bezard, R., Fischer-Gödde, M., Hamelin, C., Brennecka, G.A., Kleine, T. (2016) The effects of magmatic processes and crustal recycling on the molybdenum stable isotopic composition of Mid-Ocean Ridge Basalts. *Earth and Planetary Science Letters* 453, 171–181. https://doi.org/10.1016/j.epsl.2016.07.056

Burkhardt, C., Hin, R.C., Kleine, T., Bourdon, B. (2014) Evidence for Mo isotope fractionation in the solar nebula and during planetary differentiation. *Earth and Planetary Science Letters* 391, 201–211. https://doi.org/10.1016/j.epsl.2014.01.037

Chen, S., Hin, R.C., John, T., Brooker, R., Bryan, B., Niu, Y., Elliott, T. (2019) Molybdenum systematics of subducted crust record reactive fluid flow from underlying slab serpentine dehydration. *Nature Communications* 10, 4773. https://doi.org/10.1038/s41467-019-12696-3

Chen, S., Sun, P., Niu, Y., Guo, P., Elliott, T., Hin, R.C. (2022) Molybdenum isotope systematics of lavas from the East Pacific Rise: Constraints on the source of enriched mid-ocean ridge basalt. *Earth and Planetary Science Letters* 578, 117283. https://doi.org/10.1016/j.epsl.2021.117283

Douglass, J., Schilling, J.-G, Kingsley, R.H., Small, C. (1995) Influence of the discovery and Shona mantle plumes on the southern Mid-Atlantic Ridge: Rare earth evidence. *Geophysical Research Letters* 22, 2893–2896. https://doi.org/10.1029/95GL02665

Douglass, J., Schilling, J.-G., Fontignie, D. (1999) Plume-ridge interactions of the Discovery and Shona mantle plumes with the southern Mid-Atlantic Ridge (40°-55°S). *Journal of Geophysical Research: Solid Earth* 104, 2941–2962. https://doi.org/10.1029/98JB02642

Freymuth, H., Vils, F., Willbold, M., Taylor, R.N., Elliott, T. (2015) Molybdenum mobility and isotopic fractionation during subduction at the Mariana arc. *Earth and Planetary Science Letters* 432, 176–186. https://doi.org/10.1016/j.epsl.2015.10.006

Gale, A., Dalton, C.A., Langmuir, C.H., Su, Y., Schilling, J.-G. (2013) The mean composition of ocean ridge basalts. *Geochemistry*, *Geophysics*, *Geosystems* 14, 489–518. https://doi.org/10.1029/2012GC004334

Goldberg, T., Gordon, G., Izon, G., Archer, C., Pearce, C.R., McManus, J., Anbar, A.D., Rehkämper, M. (2013) Resolution of inter-laboratory discrepancies in Mo isotope data: an intercalibration. *Journal of Analytical Atomic Spectrometry* 28, 724–735. https://doi.org/10.1039/c3ja30375f

Greaney, A.T., Rudnick R.L., Romaniello, S.J., Anbar, A.D. (2018) Completing the Molybdenum Isotope Mass Balance in Subduction Zones. *Goldschmidt Abstracts* 872. https://goldschmidtabstracts.info/abstracts/abstractView?id=2018001568

Greaney, A.T., Rudnick, R.L., Romaniello, S.J., Johnson, A.C., Gaschnig, R.M., Anbar, A.D. (2020) Molybdenum isotope fractionation in glacial diamictites tracks the onset of oxidative weathering of the continental crust. *Earth and Planetary Science Letters* 534, 116083. https://doi.org/10.1016/j.epsl.2020.116083

Greber, N.D., Siebert, C., Nägler, T.F., Pettke, T. (2012) $\delta^{98/95}$Mo values and Molybdenum Concentration Data for NIST SRM 610, 612 and 3134: Towards a Common Protocol for Reporting Mo Data. *Geostandards and Geoanalytical Research* 36, 291–300. https://doi.org/10.1111/j.1751-908X.2012.00160.x

Greber, N.D., Pettke, T., Nägler, T.F. (2014) Magmatic–hydrothermal molybdenum isotope fractionation and its relevance to the igneous crustal signature. *Lithos* 190–191, 104–110. https://doi.org/10.1016/j.lithos.2013.11.006

Hamelin, C., Dosso, L., Hanan, B.B., Moreira, M., Kositsky, A.P., Thomas, M.Y. (2011) Geochemical portray of the Pacific Ridge: New isotopic data and statistical techniques. *Earth and Planetary Science Letters* 302, 154–162. https://doi.org/10.1016/j.epsl.2010.12.007

Kelley, K.A., Kingsley, R., Schilling, J.-G. (2013) Composition of plume-influenced mid-ocean ridge lavas and glasses from the Mid-Atlantic Ridge, East Pacific Rise, Galápagos Spreading Center, and Gulf of Aden. *Geochemistry*, *Geophysics*, *Geosystems* 14, 223–242. https://doi.org/10.1002/ggge.20049

König, S., Rosca, C., Kurzawa, T., Varas-Reus, M.I., Dragovic, B., Schoenberg, R., John, T. (2021) Selenium isotope evidence for pulsed flow of oxidative slab fluids. *Geochemical Perspectives Letters* 17, 27–32. https://doi.org/10.7185/geochemlet.2110

Labidi, J., Cartigny, P., Moreira, M. (2013) Non-chondritic sulphur isotope composition of the terrestrial mantle. *Nature* 501, 208–211. https://doi.org/10.1038/nature12490

le Roux, P., le Roex, A., Schilling, J.-G. (2002a) Crystallization processes beneath the southern Mid-Atlantic Ridge (40–55°S), evidence for high-pressure initiation of crystallization. *Contributions to Mineralogy and Petrology* 142, 582–602. https://doi.org/10.1007/s00410-001-0312-y

le Roux, P., le Roex, A., Schilling, J.G. (2002b) MORB melting processes beneath the southern Mid-Atlantic Ridge (40–55°S): a role for mantle plume-derived pyroxenite. *Contributions to Mineralogy and Petrology* 144, 206–229. https://doi.org/10.1007/s00410-002-0376-3

le Roux, P.J., le Roex, A.P., Schilling, J.G., Shimizu, N., Perkins, W.W., Pearce, N.J.G. (2002c) Mantle heterogeneity beneath the southern Mid-Atlantic Ridge: trace element evidence for contamination of ambient asthenospheric mantle. *Earth and Planetary Science Letters* 203, 479–498. https://doi.org/10.1016/S0012-821X(02)00832-4

Liang, Y.-H., Halliday, A.N., Siebert, C., Fitton, J.G., Burton, K.W., Wang, K.-L., Harvey, J. (2017) Molybdenum isotope fractionation in the mantle. *Geochimica et Cosmochimica Acta* 199, 91–111. https://doi.org/10.1016/j.gca.2016.11.023

Lyons, T.W., Reinhard, C.T., Planavsky, N.J. (2014) The rise of oxygen in Earth's early ocean and atmosphere. *Nature* 506, 307–315. https://doi.org/10.1038/nature13068

McCoy-West, A.J., Chowdhury, P., Burton, K.W., Sossi, P., Nowell, G.M., Fitton, J.G., Kerr, A.C., Cawood, P.A., Williams, H.M. (2019) Extensive crustal extraction in Earth's early history inferred from molybdenum isotopes. *Nature Geoscience* 12, 946–951. https://doi.org/10.1038/s41561-019-0451-2

Moreira, M., Staudacher, T., Sarda, P., Schilling, J.-G., Allègre, C.J. (1995) A primitive plume neon component in MORB: The Shona ridge-anomaly, South Atlantic (51–52°S). *Earth and Planetary Science Letters* 133, 367–377. https://doi.org/10.1016/0012-821X(95)00080-V

Nebel-Jacobsen, Y., Wille, M., Ivanic, T., Nebel, O. (2021) Molybdenum isotope systematics in cumulate rock of the 2.8 Windimurra layered intrusion: A test for igneous differentiation and the composition of the Archean mantle. *Precambrian Research* 355, 106087. https://doi.org/10.1016/j.precamres.2020.106087

Plank, T. (2014) 4.17 - The Chemical Composition of Subducting Sediments. In: Holland, H.D., Turekian, K.K. (Eds.) *Treatise on Geochemistry*. Second Edition, Elsevier, Oxford, 607–629. https://doi.org/10.1016/B978-0-08-095975-7.00319-3

Rehkämper, M., Hofmann, A.W. (1997) Recycled ocean crust and sediment in Indian Ocean MORB. *Earth and Planetary Science Letters* 147, 93–106. https://doi.org/10.1016/S0012-821X(97)00009-5

Rudnick, R.L., Gao, S. (2014) 4.1 - Composition of the Continental Crust. In: Holland, H.D., Turekian, K.K. (Eds.) *Treatise on Geochemistry*. Second Edition, Elsevier, Oxford, 1–51. https://doi.org/10.1016/B978-0-08-095975-7.00301-6

Salters, V.J.M., Stracke, A. (2004) Composition of the depleted mantle. *Geochemistry, Geophysics, Geosystems* 5, Q05B07. https://doi.org/10.1029/2003GC000597

Sarda, P., Moreira, M., Staudacher, T., Schilling, J.-G., Allègre, C.J. (2000) Rare gas systematics on the southernmost Mid-Atlantic Ridge: Constraints on the lower mantle and the Dupal source. *Journal of Geophysical Research: Solid Earth* 105, 5973–5996. https://doi.org/10.1029/1999JB900282

Siebert, C., Nägler, T.F., Kramers, J.D. (2001) Determination of molybdenum isotope fractionation by double-spike multicollector inductively coupled plasma mass spectrometry. *Geochemistry, Geophysics, Geosystems* 2, 2000GC000124. https://doi.org/10.1029/2000GC000124

Stracke, A. (2012) Earth's heterogeneous mantle: A product of convection-driven interaction between crust and mantle. *Chemical Geology* 330–331, 274–299. https://doi.org/10.1016/j.chemgeo.2012.08.007

Voegelin, A.R., Pettke, T., Greber, N.D., von Niederhäusern, B., Nägler, T.F. (2014) Magma differentiation fractionates Mo isotope ratios: Evidence from the Kos Plateau Tuff (Aegean Arc). *Lithos* 190–191, 440–448. https://doi.org/10.1016/j.lithos.2013.12.016

Vollmer, R. (1976) Rb-Sr and U-Th-Pb systematics of alkaline rocks: the alkaline rocks from Italy. *Geochimica et Cosmochimica Acta* 40, 283–295. https://doi.org/10.1016/0016-7037(76)90205-2

Wang, Z., Becker, H. (2018) Molybdenum partitioning behavior and content in the depleted mantle: Insights from Balmuccia and Baldissero mantle tectonites (Ivrea Zone, Italian Alps). *Chemical Geology* 499, 138–150. https://doi.org/10.1016/j.chemgeo.2018.09.023

Willbold, M., Elliott, T. (2017) Molybdenum isotope variations in magmatic rocks. *Chemical Geology* 449, 253–268. https://doi.org/10.1016/j.chemgeo.2016.12.011

Willbold, M., Hibbert, K., Lai, Y.-J., Freymuth, H., Hin, R.C., Coath, C., Vils, F., Elliott, T. (2016) High-Precision Mass-Dependent Molybdenum Isotope Variations in Magmatic Rocks Determined by Double-Spike MC-ICP-MS. *Geostandards and Geoanalytical Research* 40, 389–403. https://doi.org/10.1111/j.1751-908X.2015.00388.x

Wille, M., Nebel, O., Van Kranendonk, M.J., Schoenberg, R., Kleinhanns, I.C., Ellwood, M.J. (2013) Mo–Cr isotope evidence for a reducing Archean atmosphere in 3.46–2.76 Ga black shales from the Pilbara, Western Australia. *Chemical Geology* 340, 68–76. https://doi.org/10.1016/j.chemgeo.2012.12.018

Wille, M., Nebel, O., Pettke, T., Vroon, P.Z., König, S., Schoenberg, R. (2018) Molybdenum isotope variations in calc-alkaline lavas from the Banda arc, Indonesia: Assessing the effect of crystal fractionation in creating isotopically heavy continental crust. *Chemical Geology* 485, 1–13. https://doi.org/10.1016/j.chemgeo.2018.02.037

Yang, J., Siebert, C., Barling, J., Savage, P., Liang, Y.-H., Halliday, A.N. (2015) Absence of molybdenum isotope fractionation during magmatic differentiation at Hekla volcano, Iceland. *Geochimica et Cosmochimica Acta* 162, 126–136. https://doi.org/10.1016/j.gca.2015.04.011

Yang, J., Barling, J., Siebert, C., Fietzke, J., Stephens, E., Halliday, A.N. (2017) The molybdenum isotopic compositions of I-, S- and A-type granitic suites. *Geochimica et Cosmochimica Acta* 205, 168–186. https://doi.org/10.1016/j.gca.2017.01.027

Ye, Y., Zhang, S., Wang, H., Wang, X., Tan, C., Li, M., Wu, C., Canfield, D.E. (2021) Black shale Mo isotope record reveals dynamic ocean redox during the Mesoproterozoic Era. *Geochemical Perspectives Letters* 18, 16–21. https://doi.org/10.7185/geochemlet.2118

Yierpan A., König S., Labidi J., Schoenberg R. (2019) Selenium isotope and S-Se-Te elemental systematics along the Pacific-Antarctic ridge: Role of mantle processes. *Geochimica et Cosmochimica Acta* 249, 199–224. https://doi.org/10.1016/j.gca.2019.01.028

Yierpan, A., König, S., Labidi, J., Schoenberg, R. (2020) Recycled selenium in hot spot–influenced lavas records ocean-atmosphere oxygenation. *Science Advances* 6, abb6179. https://doi.org/10.1126/sciadv.abb6179

Yierpan A., Redlinger J., König S., (2021) Selenium and tellurium in Reykjanes Ridge and Icelandic basalts: Evidence for degassing-induced Se isotope fractionation. *Geochimica et Cosmochimica Acta* 313, 155–172. https://doi.org/10.1016/j.gca.2021.07.029

Zhao, P.-P., Li, J., Zhang, L., Wang, Z.-B., Kong, D.-X., Ma, J.-L., Wei, G.-J., Xu, J.-F. (2016) Molybdenum Mass Fractions and Isotopic Compositions of International Geological Reference Materials. *Geostandards and Geoanalytical Research* 40, 217–226. https://doi.org/10.1111/j.1751-908X.2015.00373.x